PROCEEDINGS OF SCIENCE

Effective field theory for $\mu \to e$ conversion in nuclei[†]

Martin Hoferichter[a,*] **and Frederic Noël**[a]

[a] *Albert Einstein Center for Fundamental Physics, Institute for Theoretical Physics, University of Bern, Sidlerstrasse 5, 3012 Bern, Switzerland*

E-mail: hoferichter@itp.unibe.ch

Observables that violate lepton flavor symmetry are sensitive probes of physics beyond the Standard Model (BSM), since any observation would be a clear BSM signal. Limits on $\mu \to e$ conversion in nuclei are amongst the most stringent ones available, and are even expected to improve by up to four orders of magnitude at Mu2e and COMET. In this contribution, we presented a general effective-field-theory analysis, including an application that shows how the spin-dependent $\mu \to e$ process already implies indirect limits on lepton-flavor-violating decays of light pseudoscalars that surpass direct limits by orders of magnitude. We also discussed the nuclear-structure input required for a robust interpretation of $\mu \to e$ conversion limits, in particular, uncertainties propagated from the nuclear charge distributions as well as uncertainty quantification for $\mu \to e$ overlap integrals.

The XVIth Quark Confinement and the Hadron Spectrum Conference (QCHSC24)
19-24 August, 2024
Cairns Convention Centre, Cairns, Queensland, Australia

[†]The contents of this work are based on Refs. [1–4], see Ref. [5] for related proceedings.
[*]Speaker

 ISSN 1824-8039 . Published by SISSA Medialab.

PoS(QCHSC24)177

LFV process	current limit	(planned) experiments
$\mu \to e\gamma$	$< 4.2 \times 10^{-13}$ [7]	MEG II [7]
$\mu \to 3e$	$< 1.0 \times 10^{-12}$ [8]	Mu3e [9]
$\tau \to \ell\gamma, 3\ell, \ell P, \ldots$	$\lesssim 10^{-8}$ [10–14]	Belle II [15], ...
$K \to \mu e, \mu e\pi, \mu e\pi\pi$	$\lesssim 10^{-11}$ [16–19]	KOTO [20], LHCb [21]
$\pi^0 \to \mu e$	$< 3.6 \times 10^{-10}$ [18, 19, 22]	JEF [24], REDTOP [25]
$\eta \to \mu e$	$< 6 \times 10^{-6}$ [23]	
$\eta' \to \mu e$	$< 4.7 \times 10^{-4}$ [26]	
Au $\mu^- \to$ Au e^-	$< 7 \times 10^{-13}$ [27]	
Ti $\mu^- \to$ Ti e^-	$< 6.1 \times 10^{-13}$ [28]	
Al $\mu^- \to$ Al e^-	$\lesssim 10^{-17}$ (projected)	Mu2e [29], COMET [30]

Table 1: A selection of LFV processes and limits on their branching ratios given at 90% confidence level. The conversion rate is normalized to the muon capture rate [31].

1. Introduction

Lepton-flavor-violating (LFV) processes are promising observables in the search for physics beyond the Standard Model (BSM), as lepton flavor is an accidental symmetry that may well be violated by BSM extensions, beyond neutral LFV observed via neutrino oscillations [6]. Thus, the consideration of LFV operators in a general effective-field-theory (EFT) manner is a natural SM extension. As the SM conserves lepton flavor (up to tiny corrections induced by neutrino oscillations), any observation would be a direct BSM signal, while improved limits put very stringent bounds on the LFV operators, which results in significant restrictions on potential BSM scenarios. An incomplete selection of current limits on LFV processes is given in Table 1.

On the one hand, the currently most stringent limits come from the purely leptonic channels $\mu \to e\gamma$ and $\mu \to 3e$ with future improvements expected from MEG II [7] and Mu3e [9], respectively. On the other hand, $\mu \to e$ conversion, see Sec. 2, probes complementary effective operators to the leptonic channels and gives similarly stringent limits on LFV, with upcoming substantial experimental improvements at Mu2e [29] and COMET [30] reaching for a precision improvement by up to four orders of magnitudes. The limits for LFV decays of light pseudo-scalars are much less stringent but could see some improvements from the planned eta factory experiments of REDTOP [25] or JEF [24]. Here, it has been shown that spin-dependent $\mu \to e$ conversion already implies significantly stronger indirect limits on these processes [1], see Sec. 3.

Due to these upcoming experimental advances in $\mu \to e$ conversion, it is timely to develop a comprehensive description of $\mu \to e$ conversion that enables robust, quantitative statements about the effective LFV operators. To describe $\mu \to e$ conversion in a model-independent way starting from the underlying LFV operators, the associated Wilson coefficients, originally defined at the high scale, need to be evolved by a concatenation of different EFTs to the low scale where the experiments are performed [1–4, 32–43]. After running the effective operators down to the electroweak scale [44–46] and integrating out the heavy SM particles, the effective quark-level operators are turned

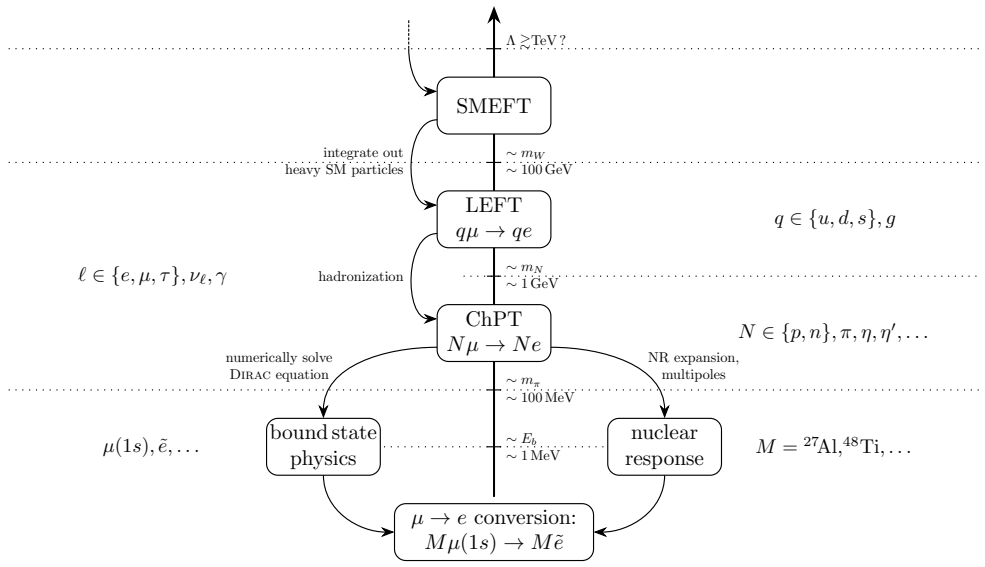

Figure 1: Schematic representation of the EFT scales for $\mu \to e$ conversion.

into hadronic operators using hadronic matrix elements, which are then embedded into nuclear responses employing nuclear matrix elements. Finally, Coulomb corrections on the leptonic side of the interaction need to be considered. The different scales and EFTs relevant for this process are illustrated in Fig. 1, leading to a description as illustrated in Fig. 2 that consists of EFT Wilson coefficients, hadronic matrix elements, nuclear matrix elements, and Coulomb corrections.

While controlling uncertainties at all steps along the way is important, a weak point, so far, concerns the nuclear matrix elements, which have been largely based on empirical models, whose uncertainties are hard to assess especially for quantities for which direct experimental validation is difficult to obtain, most notably, nuclear responses related to neutron distributions. Only recently experimental measurements of parity-violating electron scattering (PVES) have become available, allowing for a test of neutron responses [47, 48]. To address these shortcomings, ab-initio nuclear-structure methods can be employed to calculate the nuclear matrix elements, implementing important properties of QCD such as chiral symmetry. In fact, the uncertainties are dominated by the considered chiral Hamiltonians and not by the many-body calculations, which suggests a correlation analysis to relate the neutron responses to their experimentally much better known proton analogs [49, 50]. In Sec. 6, we report on the application of this method to provide results for the so-called overlap integrals in $\mu \to e$ conversion defined in Sec. 4, which combine nuclear responses and Coulomb corrections, based on nuclear charge distributions extracted from elastic electron–nucleus scattering, including quantified uncertainties, see Sec. 5.

Figure 2: Schematic representation of the components of the EFT framework for $\mu \to e$ conversion.

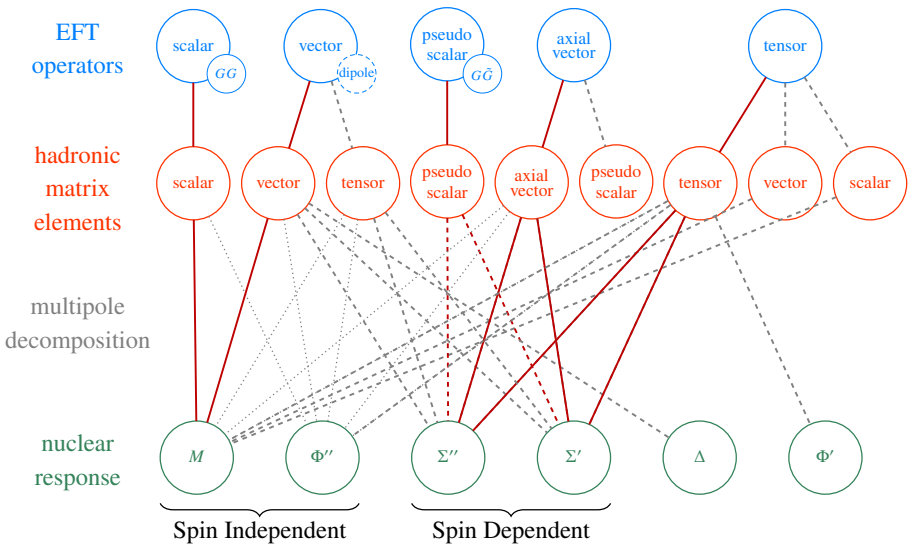

Figure 3: Decomposition of the hadronic side of $\mu \to e$ conversion from the EFT operators to the resulting nuclear responses. Dashed lines are suppressed by q/m_N, dotted lines by q^2/m_N^2.

2. $\mu \to e$ conversion in nuclei

$\mu \to e$ conversion in nuclei refers to the process in which a muon bound to a nucleus in the $1s^{1/2}$ ground state converts into an electron without emitting neutrinos. Since, up to a small recoil of the nucleus, the mass of the muon is converted into kinetic energy of the electron, the electron will then be ejected from the nucleus, while its wave function is distorted by the nucleus potential. On the quark level, this process can happen either via a variety of point interactions with the quarks and gluons in the nucleus or via a long-distance one-photon exchange. The latter one we call the dipole interaction, which is also probed by $\mu \to e\gamma$. The point interactions always occur between two leptons and two of the same quarks or gluons, and thus are not probed at tree level by the leptonic channels. The full Lagrangian relevant for $\mu \to e$ conversion below the electroweak scale up to dimension 7 can be written as

$$\begin{aligned}\mathcal{L}_{\text{eff}}^{\mu\to e} = \frac{1}{\Lambda^2}\sum_{Y=L,R}\Bigg(&\Lambda C_Y^D \overline{e_Y}\sigma^{\mu\nu}\mu F_{\mu\nu} + C_Y^{GG}\frac{\alpha_s}{\Lambda}\overline{e_Y}\mu\, G^a_{\alpha\beta}G_a^{\alpha\beta} + C_Y^{G\tilde{G}}\frac{i\alpha_s}{\Lambda}\overline{e_Y}\mu\, G^a_{\alpha\beta}\tilde{G}_a^{\alpha\beta}\\ &+ \sum_{q=u,d,s}\Big[\overline{e_Y}\mu\Big(C_Y^{S,q}\bar{q}q + C_Y^{P,q}\bar{q}\gamma_5 q\Big) + \overline{e_Y}\gamma^\mu\mu\Big(C_Y^{V,q}\bar{q}\gamma_\mu q + C_Y^{A,q}\bar{q}\gamma_\mu\gamma_5 q\Big)\\ &+ C_Y^{T,q}\overline{e_Y}\sigma^{\mu\nu}\mu\,\bar{q}\sigma_{\mu\nu}q\Big] + \text{h.c.}\Bigg),\end{aligned} \tag{1}$$

with the labels referring to scalar (S), pseudo-scalar (P), vector (V), axial-vector (A), tensor (T), dipole (D), and the gluon structure, respectively. These quark-level interactions then couple to nucleons via hadronic matrix elements, which finally map onto different nuclear responses via a multipole decomposition. Figure 3 shows how the hadronic part of the different effective operators ultimately contributes to the different nuclear responses, following the procedure of Fig. 1, see

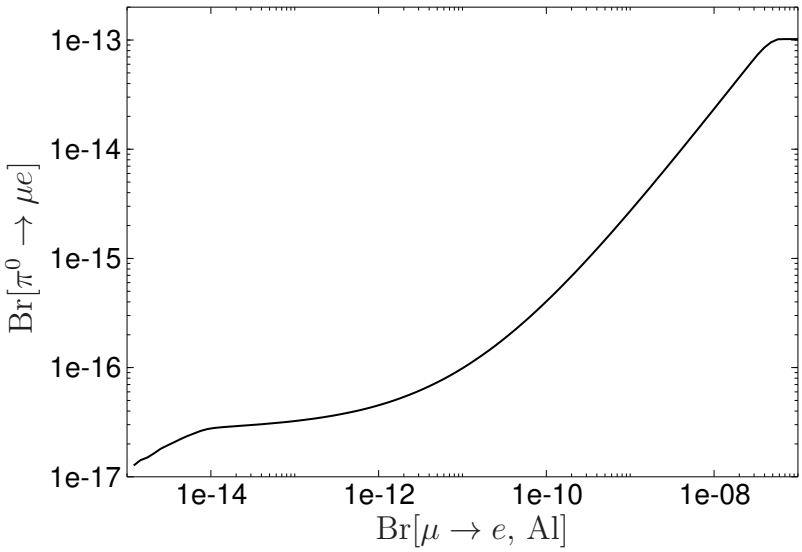

Figure 4: Projection for $\mathrm{Br}[\pi^0 \to \mu e]$ as a function of a future limit for the $\mu \to e$ branching fraction in ^{27}Al and the current limit for ^{48}Ti [28]. In the limit in which the ^{27}Al constraint disappears, one obtains $\mathrm{Br}[\pi^0 \to \mu e] < 1.2 \times 10^{-13}$ [1].

Ref. [3]. At leading order, one distinguishes between spin-independent (SI) and spin-dependent (SD) responses. The former show a coherent enhancement with the number of nucleons in the nucleus, so that the conversion rate scales with $\#N^2$, where $\#N$ is Z for proton responses and $A - Z$ for neutron responses. SD interactions only exist for nuclei with non-zero total nucleus spin and are not coherently enhanced. This also means that experimental limits imply much more stringent constraints on SI than on SD interactions.

The leading SI interactions originate from scalar, vector, and dipole operators, as can be deduced from Fig. 3. The resulting SI $\mu \to e$ conversion rate is conventionally expressed in terms of so-called overlap integrals [32], according to

$$\mathrm{Br}^{\mathrm{SI}}_{\mu\to e} = \frac{4m_\mu^5}{\Gamma_{\mathrm{cap}}} \sum_{Y=L,R} \left| \bar{C}_Y^D D + \sum_{N=p,n} \left[\bar{C}_Y^{S^{(N)}} S^{(N)} + \bar{C}_Y^{V^{(N)}} V^{(N)} \right] \right|^2, \tag{2}$$

with the muon capture rate Γ_{cap}. The overlap integrals $S^{(N)}$, $V^{(N)}$, and D combine the inputs from the nuclear responses and the Coulomb corrections, see Sec. 4. The prefactors are given by

$$\bar{C}_Y^{S^{(N)}} = \frac{1}{\Lambda^2} \sum_q C_Y^{S,q} \frac{m_N}{m_q} f_q^N + \frac{4\pi}{\Lambda^3} C_Y^{GG} a_N, \qquad \bar{C}_Y^{V^{(N)}} = \frac{1}{\Lambda^2} \sum_q C_Y^{V,q} f_{V_q}^N, \qquad \bar{C}_Y^D = \frac{\eta_e}{4m_\mu \Lambda} C_Y^D, \tag{3}$$

where f_q^N, a_N, $f_{V_q}^N$, η_e refer to hadronic matrix elements and phase factors, see Refs. [1, 3, 51–53].

3. Pseudo-scalar decays

A similar master formula as Eq. (2) can also be derived for the SD case and for the meson decays $\pi^0, \eta, \eta' \to \mu e$. One then observes that these processes depend on the same set of Wilson

coefficients, so that limits on one process imply limits on the other. This connection becomes particularly robust in the case of the π^0, in which case a rigorous limit can be derived when scanning over the entire space of Wilson coefficients, see Fig. 4, orders of magnitude better than the direct limit. For η, η', the general sensitivity also improves by many orders of magnitude over direct limits, but flat directions in parameter space do exist. In those cases, however, already RG corrections and the resulting connection to SI limits all but exclude such scenarios.

4. Overlap integrals

The overlap integrals combine the nuclear responses with the Coulomb corrections and are given for dipole, scalar, and vector interactions as appearing in Eq. (2) as [32]

$$\begin{aligned} D^{(N)} &= -\frac{4}{\sqrt{2}\, m_\mu^{3/2}} \int_0^\infty \mathrm{d}r\, E(r) \left[g_{-1}^e(r)\, f_{-1}^\mu(r) + f_{-1}^e(r)\, g_{-1}^\mu(r) \right], \\ S^{(N)} &= \frac{\#N}{2\sqrt{2}\, m_\mu^{5/2}} \int_0^\infty \mathrm{d}r\, \rho_N(r) \left[g_{-1}^e(r)\, g_{-1}^\mu(r) - f_{-1}^e(r)\, f_{-1}^\mu(r) \right], \\ V^{(N)} &= \frac{\#N}{2\sqrt{2}\, m_\mu^{5/2}} \int_0^\infty \mathrm{d}r\, \rho_N(r) \left[g_{-1}^e(r)\, g_{-1}^\mu(r) + f_{-1}^e(r)\, f_{-1}^\mu(r) \right], \end{aligned} \tag{4}$$

with $N = p, n$ and the electric field given by

$$E(r) = \frac{\sqrt{4\pi\alpha_{\mathrm{el}}}}{r^2} \int_0^r \mathrm{d}r'\, r'^2 \rho_{\mathrm{ch}}(r'), \tag{5}$$

in terms of the nuclear charge distribution $\rho_{\mathrm{ch}}(r)$. The weights $\rho_p(r)$ and $\rho_n(r)$ are the point-proton and point-neutron distributions of the nucleus and are directly related to the M multipole responses. In this way, the first factor in the integrals constitutes the nuclear-response contribution to $\mu \to e$ conversion. The latter factor is determined by lepton wave functions f_κ^ℓ, g_κ^ℓ, $\ell = e, \mu$, obtained via the solution of the Dirac equation for the charge potential of the nucleus, see Refs. [2, 3] for details. In this way, the full Coulomb corrections beyond a plane-wave approximation are implemented.

One observes that the charge distribution of the nucleus ρ_{ch} is crucial at several points of the calculation of the overlap integrals. First, the charge distribution defines the electric field according to Eq. (5), which is directly required for the dipole overlap integral D. Second, the electric field defines the nucleus potential used to calculate the muon and electron wave functions. Finally, in Sec. 6 we will show that also improved input for the point-proton and point-neutron distributions can be deduced from the charge distribution using correlations established from ab-initio calculations. Hence, reliable input for the charge distribution, including uncertainty quantification, is crucial for the $\mu \to e$ overlap integrals.

5. Charge distributions

In the previous section, we have shown the importance of precise nuclear charge distributions for the calculation of overlap integrals to assess uncertainties of the overlap integrals. Unfortunately, most of the currently available model-independent parameterizations do not include such uncertainty

quantification [54]. For this reason, we revisited the extraction of the charge distributions from electron–nucleus scattering data, to try and propagate the experimental uncertainties and assess the truncation errors when assuming a given parameterization. The differential cross section for $e^-(k) + M(p) \to e^-(k') + M(p')$, the scattering of electrons off a nucleus M, is often written as

$$\frac{\mathrm{d}\sigma}{\mathrm{d}\Omega} = \left(\frac{\mathrm{d}\sigma}{\mathrm{d}\Omega}\right)_{\text{Mott}} \times \frac{E_e'}{E_e} \times \left|F(q,\theta)\right|^2, \tag{6}$$

with momentum transfer $\bar{q}_\mu = k'_\mu - k_\mu = p_\mu - p'_\mu$ and $q = |\mathbf{q}|$. In the plane-wave Born approximation (PWBA), the form factor can be further decomposed into longitudinal, $F_L(q)$, and transverse, $F_T(q)$, components

$$\left|F(q,\theta)\right|^2 = \left|F_L(q)\right|^2 + \left(\frac{1}{2} + \tan^2\frac{\theta}{2}\right)\left|F_T(q)\right|^2, \tag{7}$$

both of which can be further expanded into pieces with definite angular momentum L

$$\left|F_L(q)\right|^2 = \sum_{L\,\text{even}\,\leq 2J} \left|ZF_L^{\text{ch}}(q)\right|^2, \qquad \left|F_T(q)\right|^2 = \sum_{L\,\text{odd}\,\leq 2J} \left|F_L^{\text{mag}}(q)\right|^2, \tag{8}$$

where J is the spin of the nucleus. The sole contribution for $J = 0$, and leading contribution in general, is the charge form factor F_0^{ch}. It is directly related to the nuclear charge distribution ρ_{ch} via the Fourier transformation

$$ZF_0^{\text{ch}}(q) = \int \mathrm{d}^3 r\ \rho(r) e^{-i\mathbf{q}\cdot\mathbf{r}} = 4\pi \int \mathrm{d}r\ r^2\, j_0(qr)\rho_{\text{ch}}(r). \tag{9}$$

Hence, if the PWBA were exact and potential higher L contributions under control, the charge distribution would be straightforward to extract from the charge form factor. Unfortunately, even for nuclei with $J = 0$, this extraction becomes complicated by Coulomb corrections. While the PWBA assumes a point-like nucleus with no extension and plane waves for the initial and final electron wave functions, in reality, the extension of the nucleus plays a key role and its potential distorts the electron wave functions. This shifts the cross section and fills out minima in the form factor, which is crucial for an accurate description of the experimental cross-section data.

To include these effects, one again solves the Dirac equation for the electron in the nucleus potential. For $L = 0$ the cross section can then be calculated using the so-called phase-shift model, which uses the asymptotic phase shift differences (compared to the point-like Coulomb problem) for the numerical solutions of the Dirac equation for the different partial waves. An efficient numerical implementation and optimization of the phase-shift model becomes important especially for the estimation of systematic effects, which requires evaluating fits many times over a large space of external parameters. For this reason, we developed the Python package `phasr`, which efficiently performs the procedure of the phase-shift model [55]. Using this package we were able to extract charge distribution parameterizations for ^{27}Al, ^{40,48}Ca, and ^{48,50}Ti including comprehensive uncertainty estimates containing statistic and systematic components [2], based on the experimental cross-section measurements and truncation uncertainties of the expansion into Fourier–Bessel series [56]. Such a parameterization allows one to represent the charge distribution and derived quantities in a largely model-independent form, as long as the sensitivity to the truncation in N and the cutoff radius R is appropriately taken into account, see Fig. 5 for some representative results.

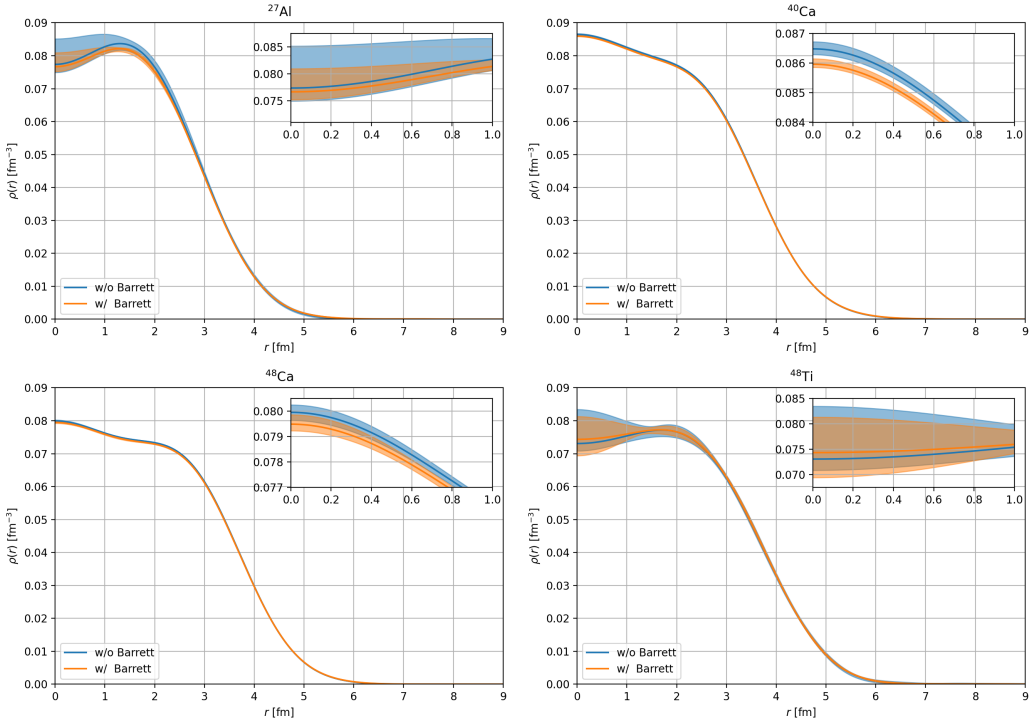

Figure 5: Charge densities of ^{27}Al, ^{40,48}Ca, and ^{48}Ti. Two variants are shown, with (orange) or without (blue) the constraints from Barrett moments as determined from muonic atom spectroscopy.

6. Correlation analysis of overlap integrals

As shown in Eq. (4), in contrast to the dipole overlap integral, the scalar and vector overlap integrals depend on the point-proton and point-neutron distributions. While the point-proton distribution is the dominating contribution to the charge density, so that only corrections need to be supplemented by nuclear-structure calculations, the neutron density is much harder to probe directly in experiment. Information on the neutron distribution can be determined using PVES or neutrino scattering [57, 58], but, at present, only a very limited amount of data is available that does not suffice to extract the neutron responses from experiment.

For this reason, one needs to employ theoretical calculations for these responses. While phenomenological models often employ approximations that need to be validated by data, current ab-initio calculations, in principle, allow one to predict the responses from few-nucleon input using chiral EFT. In practice, results can still display considerable uncertainties related to EFT truncations and scheme dependence of the chiral Hamiltonian. However, in many cases, the correlation between the neutron responses and experimental observables, such as the charge radius, proves much more robust than the chiral prediction of the neutron responses themselves, which makes it possible to improve the calculation via such a correlation analysis [49, 50]. This strategy also applies directly to the overlap integrals that depend on point-proton and point-neutron densities, see Sec. 5 and Ref. [2], for which we could establish correlations using a wide range of chiral schemes and orders, see Fig. 6. The many-body calculations are performed using the (valence-space) in-medium similarity renormalization group, (VS-)IMSRG [59–63], with chiral interactions from Refs. [64–68].

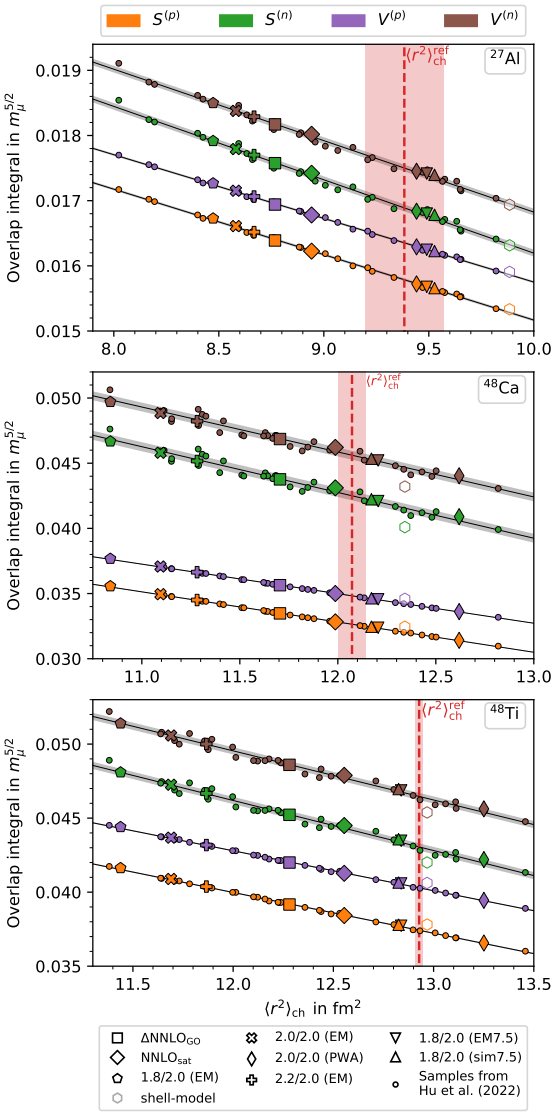

	I_i	This work/[2, 4]	[32]
^{27}Al	D	0.0359(2)	0.0362
	$S^{(p)}$	0.01579(2)(19)	0.0155
	$S^{(n)}$	0.01689(5)(21)	0.0167
	$V^{(p)}$	0.01635(2)(18)	0.0161
	$V^{(n)}$	0.01750(5)(21)	0.0173
^{48}Ca	D	0.07479(10)	–
	$S^{(p)}$	0.03265(03)(16)	–
	$S^{(n)}$	0.04250(34)(25)	–
	$V^{(p)}$	0.03483(02)(16)	–
	$V^{(n)}$	0.04561(34)(24)	–
^{48}Ti	D	0.08640(11)	0.0864
	$S^{(p)}$	0.03742(05)(5)	0.0368
	$S^{(n)}$	0.04305(25)(6)	0.0435
	$V^{(p)}$	0.04029(04)(5)	0.0396
	$V^{(n)}$	0.04646(24)(5)	0.0468

Figure 6: Left: Correlations between the charge radius and the overlap integrals, using the (VS-)IMSRG based on a representative set of chiral Hamiltonians. Right: Resulting overlap integrals. The values for the dipole overlap integral D are reproduced from Ref. [2], with the therein quoted total uncertainty. The other overlap integrals are taken from Ref. [4], where the first uncertainty quantifies the remaining nuclear-structure uncertainties based on the correlation, and the second one is propagated from the reference value of $\langle r^2 \rangle_{\rm ch}$ [2].

In Fig. 6, we consider the isotopes ^{27}Al and ^{48}Ti due to their relevance for $\mu \to e$ conversion, as well as ^{48}Ca as an important benchmark for nuclear-structure calculations with direct application to PVES. The figure shows the correlations between the scalar and vector overlap integrals and the charge radius squared, which are all well described by a simple linear regression. It also lists the resulting values for the overlap integrals. We estimate the fit uncertainty from the distribution of the fit residuals and propagate correlations among the resulting overlap integrals from the residual distributions of the different fits. As a second uncertainty component, we propagate the uncertainties and correlations coming from the reference charge radius squared, see Ref. [4] for more details.

7. Conclusions

For a systematic study of LFV operators from $\mu \to e$ conversion, controlling uncertainties for all contributions to the conversion rate is crucial. In particular, the accuracy of nuclear responses is hard to quantify, and Coulomb corrections further complicate the situation. We have shown that reliable uncertainty estimates for nuclear charge distributions play an important role in tackling these problems, summarizing the results of Ref. [2], in which we revisited their determination from electron–nucleus scattering. These charge distributions could then be used to calculate the overlap integrals for $\mu \to e$ conversion including uncertainty estimates. For the dipole operator, the transition is immediate, while for the scalar and vector overlap integrals a correlation analysis is required that relates proton and, especially, neutron densities to the charge radius, as established from ab-initio calculation in the (VS-)IMSRG [4]. These overlap integrals constitute the main result of this work, combining the nuclear responses and Coulomb corrections necessary for a systematic study of the SI $\mu \to e$ conversion rate. The generalization to SD responses is in progress.

Acknowledgments

We would like to thank Javier Menéndez for providing shell-model calculations and collaboration on Ref. [1], as well as Matthias Heinz, Takayuki Miyagi, and Achim Schwenk for ab-initio calculations using the (VS-)IMSRG and collaboration on Ref. [4]. Financial support by the SNSF (Project No. TMCG-2_213690) is gratefully acknowledged.

References

[1] M. Hoferichter, J. Menéndez, and F. Noël, Phys. Rev. Lett. **130**, 131902 (2023).

[2] F. Noël and M. Hoferichter, J. High Energy Phys. **08**, 052 (2024).

[3] F. Noël, Ph.D. thesis, Bern U. (2024).

[4] M. Heinz *et al.*, (2024), arXiv:2412.04545 [nucl-th].

[5] F. Noël and M. Hoferichter, PoS **CD2024**, 109 (2025).

[6] Y. Fukuda *et al.* (Super-Kamiokande), Phys. Rev. Lett. **81**, 1562 (1998).

[7] A. M. Baldini *et al.* (MEG), Eur. Phys. J. C **76**, 434 (2016), **78**, 380 (2018).

[8] U. Bellgardt *et al.* (SINDRUM), Nucl. Phys. B **299**, 1 (1988).

[9] K. Arndt *et al.* (Mu3e), Nucl. Instrum. Meth. A **1014**, 165679 (2021).

[10] B. Aubert *et al.* (BaBar), Phys. Rev. Lett. **98**, 061803 (2007), **104**, 021802 (2010).

[11] Y. Miyazaki *et al.* (Belle), Phys. Lett. B **648**, 341 (2007), **692**, 4 (2010), **719**, 346 (2013).

[12] K. Hayasaka *et al.*, Phys. Lett. B **687**, 139 (2010).

[13] A. Abdesselam *et al.* (Belle), J. High Energy Phys. **10**, 19 (2021).

[14] N. Tsuzuki *et al.* (Belle), J. High Energy Phys. **06**, 118 (2023).

[15] W. Altmannshofer *et al.* (Belle-II), PTEP **2019**, 123C01 (2019).

[16] D. Ambrose *et al.* (BNL), Phys. Rev. Lett. **81**, 5734 (1998).

[17] A. Sher *et al.*, Phys. Rev. D **72**, 012005 (2005).

[18] E. Abouzaid *et al.* (KTeV), Phys. Rev. Lett. **100**, 131803 (2008).

[19] E. Cortina Gil *et al.* (NA62), Phys. Rev. Lett. **127**, 131802 (2021).

[20] K. Aoki *et al.*, (2021), arXiv:2110.04462 [nucl-ex].

[21] G. Anzivino *et al.*, Eur. Phys. J. C **84**, 377 (2024).

[22] R. Appel *et al.*, Phys. Rev. Lett. **85**, 2450 (2000), **85**, 2877 (2000).

[23] D. B. White *et al.*, Phys. Rev. D **53**, 6658 (1996).

[24] L. Gan *et al.*, `https://www.jlab.org/exp_prog/proposals/14/PR12-14-004.pdf`.

[25] J. Elam *et al.* (REDTOP), (2022), arXiv:2203.07651.

[26] R. A. Briere *et al.* (CLEO), Phys. Rev. Lett. **84**, 26 (2000).

[27] W. H. Bertl *et al.* (SINDRUM II), Eur. Phys. J. C **47**, 337 (2006).

[28] P. Wintz, Conf. Proc. C **980420**, 534 (1998).

[29] L. Bartoszek *et al.* (Mu2e), (2014), arXiv:1501.05241.

[30] R. Abramishvili *et al.* (COMET), Prog. Theor. Exp. Phys. **2020**, 033C01 (2020).

[31] T. Suzuki, D. F. Measday, and J. P. Roalsvig, Phys. Rev. C **35**, 2212 (1987).

[32] R. Kitano, M. Koike, and Y. Okada, Phys. Rev. D **66**, 096002 (2002).

[33] V. Cirigliano, R. Kitano, Y. Okada, and P. Tuzon, Phys. Rev. D **80**, 013002 (2009).

[34] A. A. Petrov and D. V. Zhuridov, Phys. Rev. D **89**, 033005 (2014).

[35] A. Crivellin, S. Najjari, and J. Rosiek, J. High Energy Phys. **04**, 167 (2014).

[36] A. Crivellin, M. Hoferichter, and M. Procura, Phys. Rev. D **89**, 093024 (2014).

[37] S. Davidson, Y. Kuno, and M. Yamanaka, Phys. Lett. B **790**, 380 (2019).

[38] E. Rule, W. C. Haxton, and K. McElvain, Phys. Rev. Lett. **130**, 131901 (2023).

[39] V. Cirigliano, K. Fuyuto, M. J. Ramsey-Musolf, and E. Rule, Phys. Rev. C **105**, 055504 (2022).

[40] W. C. Haxton *et al.*, Phys. Rev. C **107**, 035504 (2023).

[41] L. Borrel, D. G. Hitlin, and S. Middleton, arXiv:2401.15025.

[42] W. Haxton *et al.*, J. High Energy Phys. **11**, 076 (2024).

[43] F. Delzanno *et al.*, (2024), arXiv:2411.13497 [hep-ph].

[44] A. Crivellin, S. Davidson, G. M. Pruna, and A. Signer, J. High Energy Phys. **05**, 117 (2017).

[45] V. Cirigliano, S. Davidson, and Y. Kuno, Phys. Lett. B **771**, 242 (2017).

[46] S. Davidson, Y. Kuno, and A. Saporta, Eur. Phys. J. C **78**, 109 (2018).

[47] D. Adhikari *et al.* (PREX, CREX), Phys. Rev. Lett. **126**, 172502 (2021), **129**, 042501 (2022).

[48] D. Androić *et al.* ($Q_{\rm weak}$), Phys. Rev. Lett. **128**, 132501 (2022).

[49] G. Hagen *et al.*, Nat. Phys. **12**, 186 (2015).

[50] C. G. Payne *et al.*, Phys. Rev. C **100**, 061304 (2019).

[51] M. Hoferichter, J. Menéndez, and A. Schwenk, Phys. Rev. D **102**, 074018 (2020).

[52] M. Hoferichter, P. Klos, J. Menéndez, and A. Schwenk, Phys. Rev. D **99**, 055031 (2019).

[53] M. Hoferichter, P. Klos, J. Menéndez, and A. Schwenk, Phys. Rev. D **94**, 063505 (2016).

[54] H. de Vries, C. W. de Jager, and C. de Vries, Atom. Data Nucl. Data Tabl. **36**, 495 (1987).

[55] F. Noël, "phasr," (2025).

[56] B. Dreher *et al.*, Nucl. Phys. A **235**, 219 (1974).

[57] M. Abdullah *et al.*, (2022), arXiv:2203.07361 [hep-ph].

[58] L. A. Ruso *et al.*, (2022), arXiv:2203.09030 [hep-ph].

[59] H. Hergert *et al.*, Phys. Rep. **621**, 165 (2016).

[60] S. R. Stroberg *et al.*, Phys. Rev. Lett. **118**, 032502 (2017).

[61] S. R. Stroberg *et al.*, Ann. Rev. Nucl. Part. Sci. **69**, 307 (2019).

[62] H. Hergert, Front. Phys. **8**, 379 (2020).

[63] M. Heinz *et al.*, arXiv:2411.16014.

[64] K. Hebeler *et al.*, Phys. Rev. C **83**, 031301 (2011).

[65] A. Ekström *et al.*, J. Phys. G **42**, 034003 (2015).

[66] W. G. Jiang *et al.*, Phys. Rev. C **102**, 054301 (2020).

[67] B. S. Hu *et al.*, Nat. Phys. **18**, 1196 (2022).

[68] P. Arthuis, K. Hebeler, and A. Schwenk, (2024), arXiv:2401.06675 [nucl-th].